DOI: 10.1002/pro.70344

RESEARCH ARTICLE



Atomistic modulation of MIF-2 structure, catalysis, and biological signaling via cysteine residues and a small molecule, Ebselen

Vinnie Widjaja¹ | Sirena M. D'Orazio¹ | Pragnya Das² | Divya T. Rajendran² | Xander Takada² | Yuanjun Shi³ | Iz Varghese¹ | Yannie Lam¹ | Nicholas DaSilva⁴ | Jimin Wang³ | Victor S. Batista³ | Vineet Bhandari² | George P. Lisi^{1,5}

Correspondence

George P. Lisi, Department of Molecular Biology, Cell Biology, & Biochemistry, Brown University, Providence, RI 02903, USA; Giuliani RNA Center, Brown University, Providence, RI 02903, USA. Email: george_lisi@brown.edu

Funding information

National Science Foundation, Grant/Award Number: GRFP 2040433; National Institutes of Health, Grant/Award Number: R01GM144451

Review Editor: Aitziber L. Cortajarena

Abstract

The macrophage migration inhibitory factor (MIF) family of cytokines comprised of the MIF and D-dopachrome tautomerase (or MIF-2) paralogs share identical tertiary and quaternary structures that contribute to their overlapping enzymatic and signaling activities. Recent investigations of MIF and MIF-2 have shown them to possess N-to-C-terminal allosteric crosstalk, but despite the similarity of this "allosteric pathway," its regulation of MIF and MIF-2 is not identical. Thus, structure alone does not preserve the precise allosteric mechanism, and additional residues that modulate MIF and MIF-2 function must be characterized. Cysteines have been identified as allosteric switches for the same biochemical functions of MIF, and small molecules targeting its N-terminal enzymatic site have affected the structure of three proximal cysteines. Ebselen is a compound that forms covalent selenylsulfide bonds with MIF cysteines and is hypothesized to destabilize and dissociate the MIF trimer into monomers. Ebselen-bound MIF also displays little-to-no catalysis or biological signaling. However, it is unclear whether Ebselen similarly affects the MIF-2 paralog, despite MIF-2 containing two related cysteines (MIF contains three). We used mutagenesis, nuclear magnetic resonance, molecular dynamics simulations, in vitro and in vivo biochemistry to investigate the mechanism of Ebselen as a modulator of MIF-2 via its cysteines. Our findings suggest that Ebselen partially disrupts the MIF-2 homotrimer, though the overall population of such a structure is <35%, even on the timescale of many hours. Ebselen does attenuate the biological functions of MIF-2, and solution structural biology captures the conformational transitions preceding the destabilized MIF-2 trimer.

KEYWORDS

allostery, inhibition, MIF, NMR

1 | INTRODUCTION

The macrophage migration inhibitory factor (MIF) and D-dopachrome tautomerase (D-DT or MIF-2) cytokines are paralogs that share \sim 35% sequence identity and a

nearly indistinguishable trimeric quaternary assembly (Merk et al., 2012). This structural similarity is believed to contribute to their overlapping enzymatic activities and interactions with the cluster of differentiation 74 (CD74) receptor. MIF and MIF-2 both play a role in

¹Department of Molecular Biology, Cell Biology, & Biochemistry, Brown University, Providence, Rhode Island, USA

²Division of Neonatology, Department of Pediatrics, Cooper University Hospital, Camden, New Jersey, USA

³Department of Chemistry, Yale University, New Haven, Connecticut, USA

⁴Proteomics Core Facility, Brown University, Providence, Rhode Island, USA

⁵Giuliani RNA Center, Brown University, Providence, Rhode Island, USA



immune cell signaling upon activation of CD74, which includes the counter-regulation of glucocorticoids, the migration and recruitment of leukocytes into infectious and inflamed sites, and the sustainment of immune cell survival through inhibition of activation-induced apoptosis (Merk et al., 2012). Overexpression of both MIF and MIF-2 can lead to chronic inflammatory conditions such as rheumatoid arthritis and asthma. Thus, MIF and MIF-2 appear to toggle between diverse activities, including proinflammatory and anti-inflammatory mechanisms.

Previously, the MIF and MIF-2 structures and several conserved functions were found to be regulated by an allosteric coupling of enzymatic activity at the N-terminus to CD74 activation at the C-terminus (Chen et al., 2021, 2023). The allosteric pathway of MIF has been exploited for small molecule inhibition, where ligand binding disrupts the crosstalk between the N- and C-termini (Lubetsky et al., 2002; Trivedi-Parmar & Jorgensen, 2018). Most MIF inhibitors target the N-terminal enzymatic site, though several molecules targeting neither the N- nor C-terminus are also known (Cho et al., 2010; Lubetsky et al., 2002; Winner et al., 2008). One such molecule, 2-phenyl-1,-2-benzoselenazol-3(2H)-one (Ebselen), was discovered to destabilize MIF through the covalent modification of its Cys80 residue, leading to a loss of enzymatic activity and eventual dissociation of the trimer (Fan et al., 2013; Ouertatani-Sakouhi et al., 2010). While many examples of small molecule stabilization of nonproductive conformational states have been reported, there has been extremely scant evidence of MIF existing in any form other than its highly stable trimer (Cooke et al., 2009; Fan et al., 2013; Merk et al., 2012; Song et al., 2022).

Ebselen-induced dissociation has never been explored in the MIF-2 paralog. Despite its similar allosteric pathway and cysteine hotspots, the MIF-2 trimer has a higher thermodynamic stability and slightly different substrate and ligand binding preferences (Chen et al., 2023; Tilstam et al., 2021). We therefore wonder whether a mechanism of action for Ebselen would translate to MIF-2 (Fan et al., 2013; Ouertatani-Sakouhi et al., 2010). Our NMR studies of the MIF-2-Ebselen complex, along with site-directed mutagenesis, reveal the predominant site of Ebselen-induced structural and functional impact to be Cys23. This site is distinct from the site of modification within MIF but plays a similar role as a structural handle for multiple biochemical functions. The other cysteine of MIF-2, Cys56, appears to be modified by Ebselen with little-to-no structural effect on the protein. NMR relaxation experiments suggest Ebselen weakens the monomer-monomer interfaces of MIF-2, despite binding distal to this region. Our biochemical assays reveal that Ebselen attenuates MIF-2 enzymatic activity in vitro and CD74 receptor activation in vivo, confirming the important regulatory role for cysteine residues in the MIF superfamily. We find the timescale of MIF-2 trimer dissociation to be on the order of days, which is considerably longer than that of MIF. Further, we suggest the mechanism of Ebselen inhibition of MIF-2 to involve disruption of protein dynamics and multiple biochemical activities as well as dissociation/aggregation of a minor population (<45%) of MIF-2 trimer. Our work provides a further understanding of the coupled functions of MIF-2 and reveals the structural aspects that precede the degradation of its trimeric structure in solution. Additionally, our analysis contributes valuable insights that support ongoing efforts to differentially target the closely related MIF and MIF-2 proteins.

2 | RESULTS

2.1 | The MIF-2 structure surrounding its cysteine residues is impacted by mutations

MIF contains three cysteine residues at positions 56, 59, and 80, only some of which are modified by Ebselen. MIF-2 contains only two cysteines (23 and 56) (Fan et al., 2013; Ouertatani-Sakouhi et al., 2010), neither of which is located within a known functional site of the protein. To determine the specific sites of Ebselen modification, three MIF-2 variants were designed-C23S, C56S, and C23S/C56S. Prior to studies of these variants with Ebselen, we used ¹H-¹⁵N NMR experiments to assess the structural impacts of the mutations themselves. The C23S variant induced a large degree of NMR chemical shift perturbations (CSPs), while those of C56S were comparatively muted (Figure S1). These data suggest that Cys23 is the more critical structural handle in MIF-2. The strongest CSPs (largest green spheres in Figure S1) surrounded the site of mutation and Cys56, the other Cys residue. This observation suggests a manner of crosstalk between the Cys sites, despite their spatial separation. Line broadening of NMR resonances (Figure S1, blue spheres) occurs at sites primarily localized to the C-terminus. Overall, Cys23 appears more critical to MIF-2 structure than Cys56, and a C23S/C56S double mutant displays a mostly additive effect on CSPs (Figure S1). Despite these local atomistic effects, the overall fold of MIF-2 remains the same, as does its secondary structure (Figure S2). Thermal stabilities of the C56S and C23S/ C56S variants are diminished, while WT and C23S have similar thermal stabilities, which is surprising given the apparent structural importance of Cys23 to MIF-2.

2.2 | Cys23 of MIF-2 is a crucial site of Ebselen modification

A prior study of MIF revealed that Ebselen modified multiple cysteine residues, though the major driver of severe structural disruption was reported to be Cys80 (Fan et al., 2013; Ouertatani-Sakouhi et al., 2010). We initially

1469896x, 2025, 11, Downloaded from https://onlinelibtarsy.wiley.com/doi/10.1002/pto-70344 by Yale University, Wiley Online Library on [18/11/2025], See the Terms and Conditions (https://onlinelibrary.wiley.com/erms-and-conditions) on Wiley Online Library for rules of use; OA articles are governed by the applicable Creative Commons Licenses

used NMR to examine Ebselen-induced structural changes at MIF-2 cysteines. Like Cys80 of MIF, Cys23 of MIF-2 is located on a solvent-exposed helix, leading us to hypothesize that Cys23 would be modified by Ebselen after incubation with WT MIF-2 or MIF-2 variants for 1 h prior to NMR data collection, as shown previously for MIF (Ouertatani-Sakouhi et al., 2010). To assist with the solubility of Ebselen and minimize NMR spectral artifacts of Ebselen precipitation during titration with MIF-2, a background of 1.5% (v/v) DMSO-d₆ was used without significantly altering MIF-2 structure (Parkins, Chen, et al., 2023). ¹H-¹⁵N transverse relaxation

optimized spectroscopy-heteronuclear single quantum coherence (TROSY-HSQC) spectral overlays of apo MIF-2 (WT and variants) and MIF-2 bound to Ebselen revealed that Ebselen induces NMR CSPs in WT MIF-2 and C56S MIF-2 (Figures 1a and S3), revealing Cys23 as a site of modification. The NMR spectral effect of Ebselen is unchanged even with longer MIF-2-Ebselen incubation times, up to 24 h, as is the extent of Ebselen-induced destabilization measured with variable temperature CD spectroscopy (Figures S2, S4). Ebselen does not induce CSPs in NMR spectra of C23S or (as expected) C23S/C56S MIF-2. The Ebselen-induced

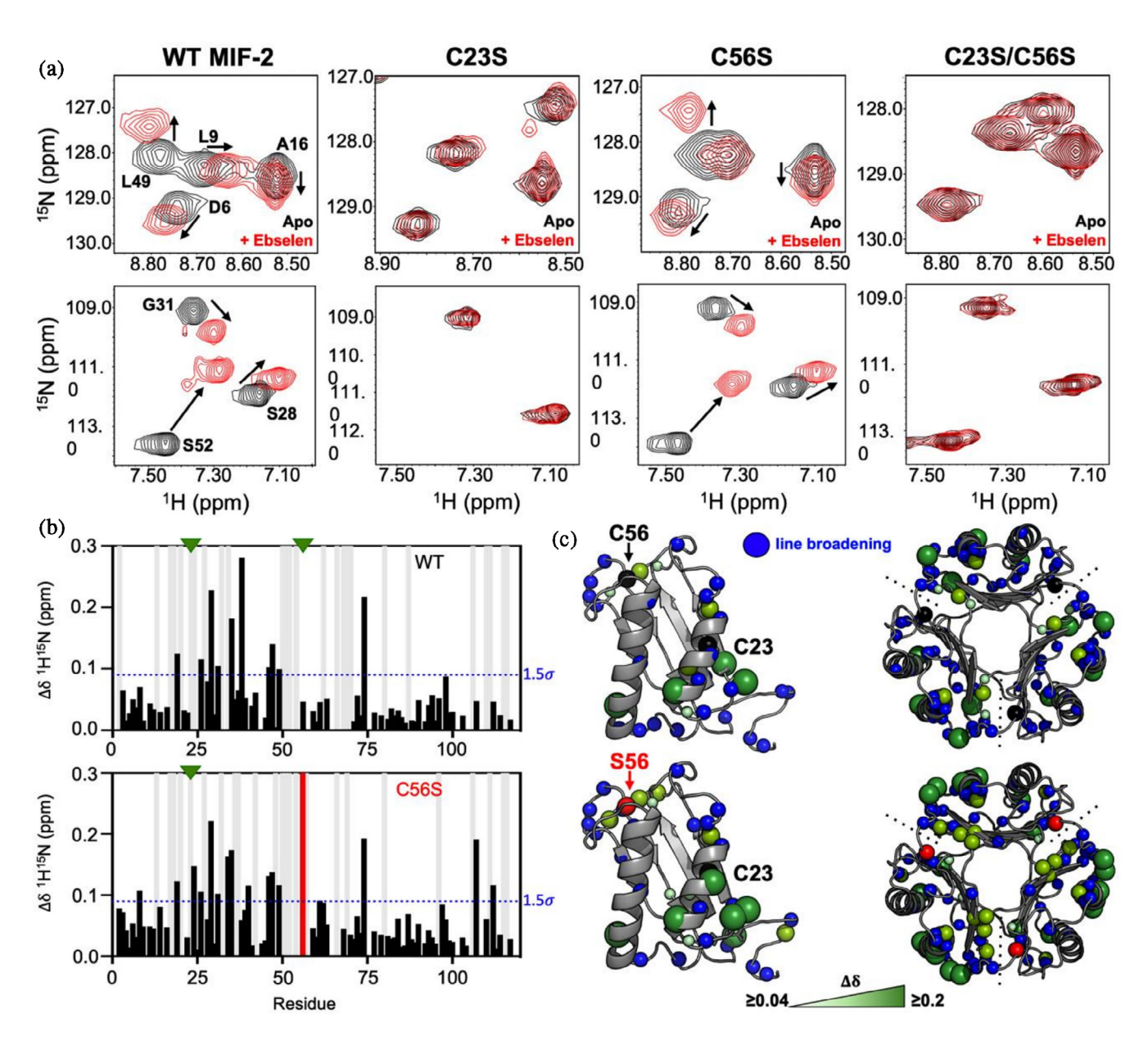


FIGURE 1 Structural effect of Ebselen on WT MIF-2 and MIF-2 variants. (a) Representative snapshots of ¹H-¹⁵N HSQC spectral overlays of apo (black) and Ebselen-bound (red) MIF-2. NMR CSPs suggest Ebselen modifies Cys23 of WT MIF-2 and the C56S variant with significant structural impact. The C23S or C23S/C56S MIF-2 variants show no evidence of structural alteration. (b) Per-residue NMR CSPs (black bars) caused by Ebselen modification of WT and C56S MIF-2. Light gray bars denote sites of NMR line broadening. The red bar denotes a Cys-to-Ser mutation, and green triangles denote a native Cys residue. (c) CSPs >1.5σ of the 10% trimmed mean of all shifts are mapped on the MIF-2 monomer (green spheres). Sphere size correlates with the intensity of the CSP. Blue spheres represent sites of NMR line broadening, red spheres denote a Cys-to-Ser mutation, and black spheres denote a native Cys residue.

CSP profiles of WT MIF-2 and C56S are very similar, localizing around Cys23 with many residues sharing the same shift trajectories, suggesting similar ligand-bound conformations (Figure 1b,c). Regions adjacent to the α helix 2 that houses Cys23 have also broadened, implying a change in its dynamics. Previously, the reduction, alkylation, or blocking of MIF cysteines by chemical cross-linking was shown to prevent Ebselen-induced MIF aggregation (Fan et al., 2013; Ouertatani-Sakouhi et al., 2010). To test a similar effect in MIF-2, we reduced its cysteines with the addition of 5 mM DTT to the NMR tube. We observed no Ebselen-induced change in the WT MIF-2 NMR spectrum or precipitation (Figure S5). Thus, Ebselen modification of MIF and MIF-2 appears to rely on redox-neutral or oxidizing conditions to modify the protein.

Due to the non-specific reactivity of Ebselen at cysteine residues, we were surprised to find little NMR evidence of modification at Cys56, located on a surfaceexposed loop. To investigate further, we performed peptide-level mass spectrometry (MS) of the MIF-2-Ebselen complex with trypsin and pepsin digestion (Ouertatani-Sakouhi et al., 2010). Two search engines (MSFragger and Spectromine) identified both unmodified and Ebselen-modified peptides. Site 1 (Cys23) peptides eluted at around 55 min, while Ebselen-modified forms appeared later (>110 min). Site 2 (Cys56), represented by the longer peptide, eluted beyond the gradient but was detected with evidence of modification, especially in the C23S mutant. Pulsar searches confirmed modification at both sites across WT MIF-2 and the variants. Pepsin digestion improved coverage (>93%) and resolution of Ebselen-modified peptides, with a +275 Da mass shift used to model Ebselen adducts (Waløen et al., 2021; Xie et al., 2022). Quantitative analysis normalized XIC areas to compare modification levels. Site 1 peptides were detected in WT and C56S variants, while Site 2 peptides were identified in WT and C23S variants. Overall, MS demonstrates that Ebselen modifies Cys23 and Cys56 of WT MIF-2, with binding restricted to Cys23 in the C56S variant and Cys56 in the C23S variant (Table S1). Challenges with these data collection included carryover and variability typical of bottom-up proteomics, which was also seen in previous MS experiments with MIF (Ouertatani-Sakouhi et al., 2010; Waløen et al., 2021; Xie et al., 2022). Thus, despite a level of modification detected by MS, we conclude that the position of Cys56 on a flexible loop near the aperture of the MIF-2 solvent channel precludes a significant structural effect by Ebselen.

2.3 | MD simulations highlight the specific contacts within MIF-2 that stabilize Ebselen

After localizing the structurally significant interaction point of Ebselen as Cys23 in MIF-2, we next

investigated the molecular contacts facilitating the complex. MD simulations generated an equilibrated structure of the MIF-2-Ebselen complex, with bond distances, bond angles, and dihedral angles consistent with the expected geometry (Table S2). A network of hydrophobic contacts surrounding the Cys23 site is observed (Figure 2a), facilitated by the aromatic rings of the Ebselen molecule. Aliphatic residues Ala24, Ala27, Ala34, Ala48, and Gly51 (backbone) comprise the major contacts, while van der Waals interactions are observed with the polar Lys20 and Thr53 residues. A comparison of unliganded MIF-2 and MIF-2-Ebselen structures reveals that Ebselen binding alters the architecture of the Cys23 pocket, especially the Ala35 and Gly51 backbone regions and the Lys20 side chain (Figure 2b). Despite these changes, the Ebselen molecule remains just outside the intersubunit cavity of adjacent MIF-2 monomers in the major conformer identified by MD. However, a second conformation clearly displays Ebselen inserted into the monomer-monomer interface, causing substantial structural perturbation (Figure 2c).

Importantly, NMR reveals a CSP or line broadening event at each of the residues shown to make contacts with Ebselen in silico, supporting the binding pose (Figure 2d). Analysis of the root-mean-square fluctuations (RMSF) surrounding the Ebselen binding site in each MIF-2 monomer reveals subtle changes to the protein dynamics (Figure S6 ΔRMSF ≤0.5 Å). Overall, Ebselen binding increases the intersubunit distances between the monomers, based on $C\alpha$ pairs at the interfaces (Figure S7). An Ebselen-induced enhancement of MIF-2 motions is therefore visible at the Cys23 binding site and monomer interfaces, consistent with NMR line broadening (Figure 2d). A similarly small, but noticeable, enhancement of MIF-2 RMSF occurs near Gly51, which is also line broadened in NMR experiments.

2.4 | Ebselen perturbs local dynamics of MIF-2, but does not disrupt the trimer on the NMR timescale

NMR spin relaxation experiments are highly sensitive to multi-timescale conformational dynamics that influence protein function and ligand binding (Lisi & Loria, 2016). These include pico-nanosecond bond vector fluctuations that organize binding sites and report on global tumbling (Wand & Sharp, 2018). We previously showed the degree of motion on this timescale to be predictive of MIF and MIF-2 catalytic function and reflect the stability of the monomer-monomer interfaces (Chen et al., 2021, 2023). To determine how Ebselen modification of MIF-2 affects its intrinsic dynamics and global tumbling, we used NMR spin relaxation. T_1 and T_2 values measured for WT MIF-2 were 1154 \pm 51 ms and 51 \pm 5 ms, respectively, consistent with prior

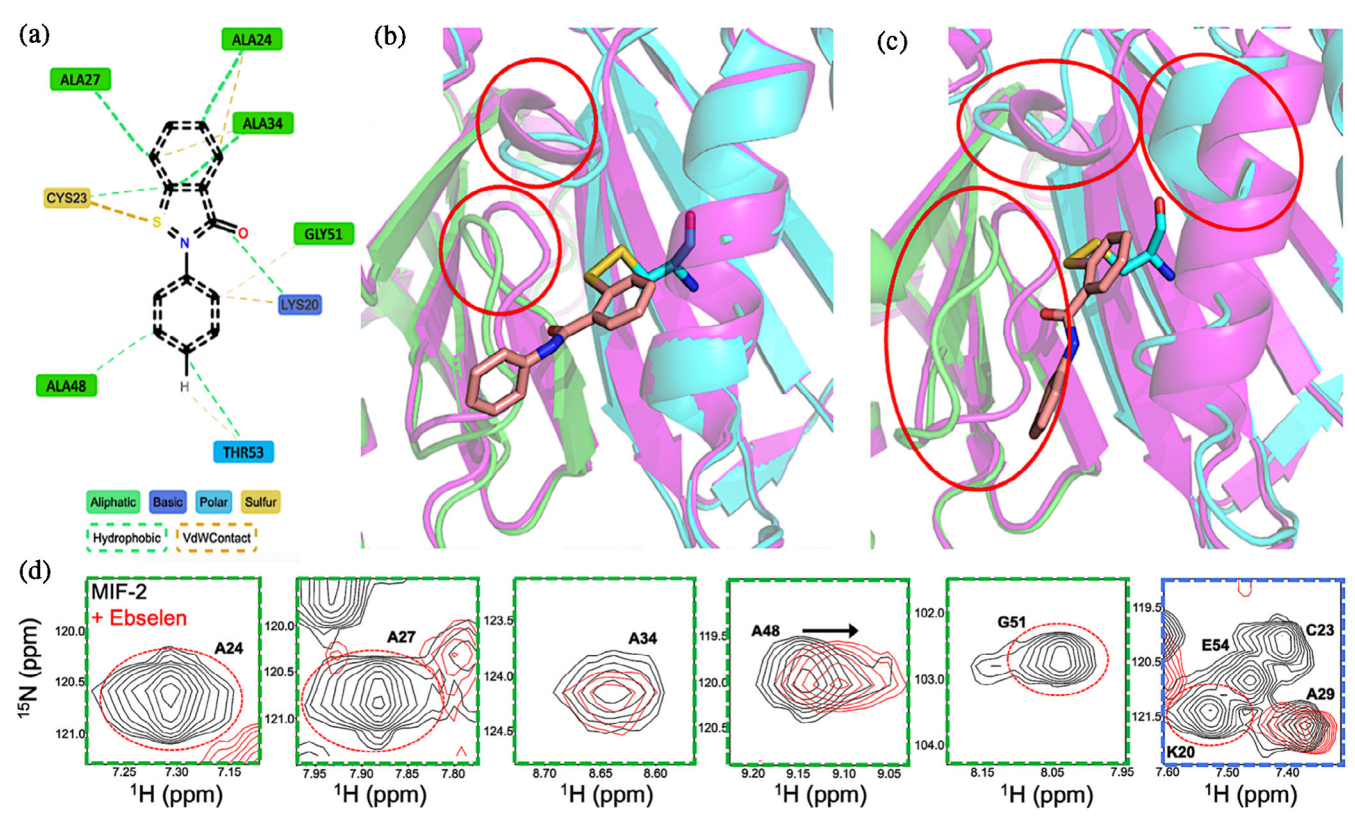


FIGURE 2 Molecular interactions between MIF-2 and Ebselen. (a) Cartoon view of MIF-2 interactions with Ebselen colored according to type. (b) A major Ebselen-bound conformation from MD simulations, where Ebselen remains outside of the intersubunit cavity (green and cyan denoting two adjacent monomers) aligned with the structure of apo MIF-2 (magenta). Major structural differences are highlighted with red circles. Ebselen is shown in tan sticks, along with its selenocysteine bond to Cys23 (gold sticks). (c) A minor conformer where Ebselen inserts into the intersubunit cavity perturbs the MIF-2 structure to a greater extent (red circles). (d) NMR suggests an interaction between MIF-2 and Ebselen at each of the residues highlighted in (a), using the same color-coded legend. A48 shows a clear CSP, while other resonances are broadened (most beyond detection, red dashed circles) in the Ebselen-bound state.

reports (Su et al., 2007). Importantly, NMR peak intensities of Ebselen-bound MIF-2 samples remained very similar over a period of 24 h (Table S3), suggesting the presence of the ligand did not complicate our ability to properly quantitate relaxation rates. The C56S variant showed similar structural compactness, with T_1 and T_2 values of 1020 ± 42 ms and 56 ± 3 ms, respectively (Table 1). When bound to Ebselen, T_1 and T_2 values for WT MIF-2 and C56S were 1142 ± 59 ms and $55 \pm 4 \text{ ms}$ and $1094 \pm 55 \text{ ms}$ and $53 \pm 4 \text{ ms}$, respectively (Table 1). These data indicate that Ebselen modification did not significantly alter the global tumbling of MIF-2. We estimated the rotational correlation times (τ_c) from these data (Kay et al., 1989), confirming that τ_{c} for Ebselen-bound forms of MIF-2 are very similar to τ_c of the apo proteins (Table 1). The calculated τ_c values are also in line with a compact protein of \sim 35 kDa (Su et al., 2007) and, importantly, suggest that Ebselen does not dissociate the MIF-2 trimer on the timescale of the NMR experiment. Though we focused on the C56S variant due to the ability of Ebselen to induce NMR CSPs, we observe a similar τ_c for free and Ebselen-bound C23S MIF-2.

TABLE 1 Effect of Ebselen on the MIF-2 molecular weight and oligomeric state.

WT MIF-2		C56S MIF-2	
(ms)	1154 ± 51	(ms)	1020 ± 42
(ms)	51 ± 5	(ms)	56 ± 3
τ_{c} (ns)	15 ± 0.4	τ_{c} (ns)	13 ± 0.4
$\mathbf{WT}\mathbf{MIF-2} + \mathbf{Ebselen}$		C56S MIF-2 + Ebselen	
(ms)	1142 ± 59	(ms)	1094 ± 55
(ms)	55 ± 4	(ms)	53 ± 4
τ_{c} (ns)	15 ± 0.7	τ_{c} (ns)	14 ± 0.5

Note: Residue-averaged T_1 and T_2 values for WT MIF-2 and C56S MIF-2 in the absence and presence of Ebselen are nearly identical. Estimated rotational correlation times (τ_c) for each state are similar and consistent with a \sim 35 kDa protein.

Though average relaxation parameters of MIF-2 appear unaffected by mutation or by Ebselen, perresidue analysis highlights differences in the flexibility of specific regions of the protein as a result of Ebselen modification. We hypothesized that the greatest perturbations to protein dynamics would occur near the

FIGURE 3 Effect of Ebselen on MIF-2 dynamics. (a) Correlation plot of R_2/R_1 relaxation rates for WT MIF-2 and WT MIF-2 + Ebselen. Points falling outside the red dashed boundaries (+1.5 σ of the 10% trimmed mean) are sites of significant motional perturbation in the presence of Ebselen, which are mapped onto MIF-2 in (b) as the magnitude of $\Delta R_2/R_1$ (Ebselen – Apo). (c) Correlation plot of R_2/R_1 relaxation rates for C56S MIF-2 and C56S MIF-2 + Ebselen. As in (a), points outside the red dashed boundaries are sites of significant motional perturbation in the presence of Ebselen, which are mapped onto MIF-2 in (d) as the magnitude of $\Delta R_2/R_1$ (Ebselen – Apo).

monomer-monomer interface, where Ebselen has been reported to destabilize MIF (Fan et al., 2013; Ouertatani-Sakouhi et al., 2010). Based on rotational correlation times (suggesting an intact trimer), dissection of residuespecific MIF-2 flexibility will reveal the changes that precede trimer dissociation, providing a window into the conformational reshuffling on the fast timescale. Correlation plots comparing R_2/R_1 relaxation rates for apo proteins (i.e., WT MIF-2 or C56S) and the respective Ebselen bound states show many residues to be affected by Ebselen (Figure 3a,c, Tables S4, S5). Residues with R_2/R_1 parameters outside of the red dashed boundaries ($+1.5\sigma$ of the 10% trimmed mean) of each plot denote significant Ebselen-induced changes in fast timescale flexibility. When mapped onto the MIF-2 structure (Figure 3b,d), these effects surround the Cys residues, particularly Cys23 on α -helix 2 that is adjacent to the monomer-monomer interface. This location is consistent with NMR CSPs and line broadening that qualitatively signifies heightened flexibility (Figures S1 and 1). The observed dynamic effects are, in this case, most strongly influenced by R_2 . Thus, regions of orange highlighted on the MIF-2 monomer in Figure 3 indicate elevated R₂ values of the Ebselen bound state, suggesting greater conformational exchange on the μs-ms timescale, while blue regions were sites where apo protein dynamics were suppressed by Ebselen. A further level of detail was obtained by examining the per-residue R₁ and R_2 values (Figure S8). Here, the effect of Ebselen was subtle, except for a notable change in R_2 occurring adjacent to the Cys23 binding site. Comparison of the WT and C56S proteins (Figure S8, Tables S6, S7) highlights a distinct effect of Ebselen on the C56S C-terminus, spanning residues I107-T115, which also have elevated R_2 values. Despite its negligible effect on the C23S MIF-2 NMR spectrum, Ebselen does impact the local flexibility of this variant, primarily via R₁ (Figure S9, Tables S8, S9). The overall motions of the

C23S variant are similar when compared to WT MIF-2, as well as in its liganded and unliganded states, consistent with the C56S variant.

2.5 | Solvent PRE reveals an effect of Ebselen at the MIF-2 monomer-monomer interface

To investigate whether the dynamics of trimer dissociation can be captured by other metrics, we used solvent paramagnetic relaxation enhancement (sPRE). The sPRE effect across the protein sequence reports on areas that are solvent accessible due to line broadening caused by the TEMPOL nitroxide radical (Purslow et al., 2020). When examining MIF-2 alone, a sPRE effect is only observed in regions that are solvent exposed in crystal structures (Figure 4a,b). When MIF-2 is bound to Ebselen, the sPRE effect is dramatically enhanced, with regions of solvent exposure again surrounding Cys23, with the monomer-monomer interface showing the largest decreases in resonance intensity (Figure 4b-d). We note, however, that residual peak intensities (IWT-IEbselen) are strongly positive across the entire MIF-2 sequence (Figure 4c), suggesting a widespread deprotection of MIF-2 from solvent. Collectively, solution NMR indicates that MIF-2 remains a trimer in the NMR tube, but that its monomermonomer interfaces are destabilized, allowing for increased solvent exposure of the MIF-2 core.

2.6 | Ebselen impacts MIF-2 biochemistry from a distance and slowly degrades the trimer

Stoichiometric concentrations of Ebselen (15 μ M) were previously shown to inhibit MIF tautomerase activity

FIGURE 4 Effect of Ebselen on solvent accessibility at the MIF-2 monomer interface. (a) Snapshot of a solvent PRE experiment showing the specific disappearance of resonances from the WT MIF-2 NMR spectrum when TEMPOL is present in the buffer (blue, while the WT MIF-2 reference spectrum is in red). (b) Intensity ratios (Itempol/Iapo) describing the per-residue effect of TEMPOL on apo WT MIF-2 (left) and WT MIF-2 bound to Ebselen (right). (c) Difference plot (I_{WT} – $I_{Ebselen}$) highlighting the substantially larger sPRE effect on Ebselen-bound MIF-2. (d) Residual intensity calculated in (c) is mapped onto the MIF-2 trimer and monomer. The strongest sPRE effect is shown for Ebselen-bound MIF-2 at the

(Ouertatani-Sakouhi et al., 2010). MIF-2 contains the same tautomerase active site with a conserved catalytic Pro1 at its N-terminus (Cooke et al., 2009). This site has been exploited as a drug discovery target, as enzymatic inhibition was shown to affect MIF and MIF-2 signaling via CD74 (Cooke et al., 2009; Parkins et al., 2021). We measured the enzymatic activity of MIF-2 and found that Ebselen diminished this function by \sim 45% (Figure 5a). We attribute the decrease in tautomerase activity to the structural changes surrounding Cys23 and the monomer interfaces that comprise the active site. Consistent with time-course NMR experiments, the impact of Ebselen on MIF-2 catalytic function is very stable over a 24 h period (Figure \$10). Ebselen also attenuated the tautomerase activity of C56S MIF-2 to nearly the same degree but did not strongly impact the activity of C23S MIF-2 (Figure S11), consistent with Cys23 being the most consequential site of Ebselen modification. In effect, Cys23, via Ebselen, can be a distal node with which to control MIF-2 function that was uncharacterized in catalytic prior work.

We next assessed the effect of Ebselen on the ability of MIF-2 to activate CD74 in vivo, via neutrophil recruitment to murine lungs (De Brauwer et al., 2002; De Lorenzi et al., 2009; Parkins, Das, et al., 2023). Following the intratracheal delivery of saline control, Ebselen control, WT MIF-2 (± Ebselen), or the C56S or C23S variant (± Ebselen), the percentage of neutrophils and total protein (a marker for pulmonary edema) were quantified from the bronchoalveolar lavage (BAL)

fluid (Figure 5b,c and S11, S12). As expected, WT MIF-2 stimulated CD74-dependent neutrophil recruitment and increased the total BAL protein levels, relative to control cases. Ebselen-bound MIF-2 showed significantly attenuated neutrophil recruitment and BAL protein, consistent with an inhibitory effect. The C56S variant displayed comparable neutrophil recruitment activity to that of WT MIF-2, reflecting the modest structural impact of this mutation on MIF-2. A complex with Ebselen again suppresses neutrophil recruitment and BAL protein levels. Interestingly, the C23S mutation alone completely suppressed neutrophil recruitment, despite the weakest mutation-induced NMR CSPs (Figure S11). We ascribe this effect to the location of Cys56 on the MIF-2 surface near (but not within) the CD74 binding interface. As a result of the large mutational effect, any further effect of Ebselen on C23S MIF-2 in these assays was negligible. Collectively, these data suggest that the structural and dynamic impacts of Ebselen binding propagate from the distal Cys23 to the MIF-2 C-terminus, where numerous residues have been shown to impact CD74 binding (Chen et al., 2023).

Though NMR suggested the soluble MIF-2-Ebselen complex to remain trimeric, we attempted to quantify any population of MIF-2 found in a precipitate. We used a time-dependent spin down assay to separate any visible precipitate, which has been shown to contain unstable monomers (Fan et al., 2013; Ouertatani-Sakouhi et al., 2010), from the MIF-2-Ebselen solution (Figure 5d). Over a period of 24 h, nearly 70% of MIF-2

FIGURE 5 Effect of Ebselen on the function of MIF-2. (a) Enzymatic tautomerase assays with a 4-HPP substrate show full activity for WT MIF-2 and WT MIF-2 in the presence of the equivalent volume of DMSO used to solubilize Ebselen (control). Incubation of MIF-2 with Ebselen attenuates enzymatic activity. A similar trend is observed for C56S MIF-2. Data are reported as mean \pm SEM (n=3 for each group). ****p <0.0001. (b) Ebselen-bound MIF-2 attenuates neutrophil recruitment in murine BAL fluid in vivo compared to MIF-2 alone, Ebselen alone, or saline control. A similar trend is observed for C56S MIF-2. Data are expressed as mean \pm SEM (n=4-5 for each group). **p <0.005; ****p <0.0001. (c) Ebselen-bound MIF-2 attenuates BAL fluid protein levels in vivo (a surrogate marker for alveolar-capillary leak and pulmonary edema) compared to MIF-2 alone, Ebselen alone, or saline control. A similar trend is observed for C56S MIF-2. Data are expressed as mean \pm SEM (n=4 for each group). *p <0.005; ***p <0.005; ****p <0.0001. (d) Spin-down assay quantifying the percent of soluble WT or C56S MIF-2 in solution over a 24 h period (light-to-dark red colors) using MIF-2 alone, MIF-2 with the equivalent volume of DMSO used to solubilize Ebselen (control), and MIF-2 with Ebselen. Data are reported as mean \pm SEM (n=4 for each group). **p <0.005; ****p <0.0001.

remains in solution, while $\sim\!30\%$ is spun out as precipitate. The dissociation of MIF-2 therefore happens quite slowly, with more than 12 h required to reduce the soluble fraction of MIF-2 by even 20%. Importantly, our assays point specifically to Ebselen as a driver of the solubility of MIF-2, as a control time course with the equivalent volume of DMSO required to deliver Ebselen has little-to-no effect on MIF-2. The same spin down assay conducted on C56S MIF-2 revealed an identical trend, albeit with a greater population of C56S ($\sim\!50\%$) found in the precipitate (Figure 5d). Surprisingly, Ebselen-induced destabilization of the trimer occurs after 6 h and remains stable

beyond that point. We attribute the more rapid and enhanced effect of Ebselen to the notable loss of thermostability of the C56S MIF-2 trimer, compared to WT MIF-2 (Figure S2), though other biophysical factors such as mutation-induced changes in hydrogen bonding or electrostatics propagated through MIF-2 may play a role. Consistent with tautomerase assays, Ebselen had only a small impact on C23S MIF-2 dissociation (via Cys56 binding) over time (Figure S13). Again, our data suggest that modification of Cys23 and disruption of the region surrounding its α -helix is the driver of MIF-2 trimer dissociation.

469896x, 2025, 1,1, Downloaded from https://onlinelibrary.wiley.com/doi/10.1002/pro.70344 by Yale University, Wiley Online Library on [18/11/2025]. See the Terms and Conditions (https://onlinelibrary.wiley.com/terms-and-conditions) on Wiley Online Library for rules of use; OA articles are governed by the applicable Creative Commons License

FIGURE 6 Cartoon scheme summarizing the effect of Ebselen on MIF-2. Modification of Cys23 by Ebselen (red molecule) induces structural and dynamic changes at the monomer-monomer interfaces, observed by NMR CSPs and solvent PRE (yellow dashed circles). At longer time points, visible protein precipitation is apparent, consistent with a disruption of the trimer structure and formation of disordered and aggregation-prone monomers.

3 | DISCUSSION

Molecular crosstalk between the N-terminal enzymatic and C-terminal CD74 activation sites of MIF and MIF-2 is a conserved feature of the trimeric assemblies, despite some subtle variations in amino acid composition (Chen et al., 2021, 2023). Recent work has expanded the allosteric network of MIF to include distal cysteine residues that toggle the MIF structure and fine-tune functional activity (Schinagl et al., 2018; Skeens, Gadzuk-Shea, et al., 2022; Skeens, Pantouris, et al., 2022). The structural similarity between MIF and MIF-2 has led to hypotheses of synergistic or compensatory functions (Coleman et al., 2008); thus, it is important to understand the molecular details of the MIF-2 paralog. Explorations of anti-inflammatory or anti-tumor therapies (Feng et al., 2020; Landgraf et al., 2020) targeting MIF identified Ebselen, a multifunctional small molecule that downregulates inflammation and protects cells from oxidative damage (Landgraf et al., 2020; Zhao & Holmgren, 2002). Ebselen has also been used as a cysteine-modifying drug in studies of redox mechanisms and protein aggregation in amyotrophic lateral sclerosis (ALS), Parkinson's disease, and cerebral ischemia (Capper et al., 2018; Landgraf et al., 2020; Zhao et al., 2002).

We used Ebselen as a probe to evaluate the structural and functional importance of MIF-2 cysteine residues and found that Ebselen covalently modifies both the MIF-2 Cys23 located on a solvent-exposed α -helix opposite the site of modification (Cys80) in MIF (Fan et al., 2013; Ouertatani-Sakouhi et al., 2010), and Cys56, within a flexible loop on the protein surface. Site-directed mutagenesis confirmed the point of modification, but also independently revealed the MIF-2 cysteines (particularly Cys23) as hotspots that altered its structure and function. NMR determined Ebselen-bound MIF-2 to remain trimeric in solution, albeit with a distorted monomer-monomer interface, and biochemistry provided evidence that trimer

destabilization and MIF-2 aggregation occurs on a timescale of several hours to days (Figure 6). However, the portion of MIF-2 rendered as an unstable precipitate (and presumably monomeric) by Ebselen represents a minor fraction (<50%), while the majority remains in solution with diminished biochemical and biological activities.

Ebselen has furthered an appreciation for the critical influence of cysteine residues on the allosterically coupled N-terminal catalytic tautomerase activity and C-terminal CD74 activation of the MIF superfamily (Chen et al., 2021, 2023; Pantouris et al., 2015, 2018). Prior work reported Cys56, Cys59, and Cys80 of MIF to each play distinct roles in its redox chemistry and structural landscape. Conformational dynamics surrounding the C₅₆-A-L-C₅₉ thioredoxin-like motif were shown to be critical for therapeutic antibody targeting of MIF (Schinagl et al., 2016; Thiele & Bernhagen, 2005), as were redox-dependent modifications of each site (Sajko et al., 2024). Mutation or modification of Cys80 was also shown to shift the MIF structural equilibrium toward a latent conformer that, when disrupted, abolished CD74 activation (Skeens, Pantouris, et al., 2022). The cysteine residues of MIF-2 have never been explored as distal modulators of function, partially because only Cys56 of MIF-2 is conserved between the proteins. Cys23, like Cys80 of MIF, is located on a solvent exposed α -helix, though on the opposite side of the monomer. Like Cys80 of MIF, our biochemical studies show that mutation of MIF-2 Cys23 diminishes catalytic function, CD74 activation, and inflammation in murine lungs. When modified with Ebselen, similar effects are observed, highlighting its contribution as a key structural node within MIF-2. While the conserved Cys56 does not induce significant structural change to MIF-2 when bound to Ebselen, its proximity to the CD74 binding region ablates this function upon mutation.

It is important to note that subtle differences between the MIF and MIF-2 trimers at the biophysical

level may differentiate their biological roles. It was recently suggested that CD74 binding and activation may be dictated by a small stretch of C-terminal residues, and many chemically similar small molecules show a preference for one paralog over another, despite their identical tertiary structures (Al-Abed et al., 2005; Tilstam et al., 2019; Xiao et al., 2022). Prior studies of the MIF-Ebselen complex showed an almost total dissociation of the MIF trimer over the course of 1 h (Fan et al., 2013; Ouertatani-Sakouhi et al., 2010) while our work with MIF-2 suggests ~35% of the total Ebselen-bound protein aggregates and precipitates after 24 h. Nonetheless, Ebselen remains the only known compound capable of disrupting this stable (~picomolar affinity) (Fan et al., 2013; Ouertatani-Sakouhi et al., 2010) and compact trimeric structure, which is widely considered to be the biologically active form.

4 | CONCLUSION

We report the cysteine residues of MIF-2 as previously unrecognized structural handles that, when modified by the small molecule Ebselen, undergo local structural changes that propagate to the interfaces of its trimer structure to disrupt its enzymatic and cellular signaling functions. Cysteine-mediated allostery within the well-studied MIF-2 paralog, MIF, was confirmed only in the past few years. Despite Ebselen-induced destabilization, a substantial portion of the MIF-2 trimer remains intact in solution, suggesting greater structural resilience compared to MIF. NMR highlights the atomic-level structural changes that prime the MIF-2 trimer for eventual dissociation, which, given the widely hypothesized pathophysiological roles of the MIF superfamily, opens new avenues for therapeutic intervention.

5 | MATERIALS AND METHODS

5.1 | Protein expression and purification

Wild-type and mutant MIF-2 was expressed and purified as previously described (Shi et al., 2006). To produce unlabeled protein for biochemical assays, a pET-22b plasmid encoding MIF-2 was transformed into BL21-Gold (DE3) *Escherichia coli* cells and grown in Luria-Bertani (LB) medium at 37°C to an OD $_{600}$ of 0.6–0.8. Protein expression was induced with 1 mM IPTG followed by shaking at 20°C for 16 h. Cells were harvested by centrifugation and resuspended in a buffer of 20 mM Tris and 20 mM NaCl at pH 8.5, supplemented with 1 mM phenylmethylsulfonyl fluoride. Cells were lysed by sonication on ice and then centrifuged to remove cell debris. The supernatant was filtered through a 0.22 μ m filter, loaded onto a Q-Sepharose

(anion-exchange) column, washed with a buffer of 20 mM Tris and 20 mM NaCl at pH 8.5, and eluted with 5% of a buffer of 20 mM Tris and 1 M NaCl at pH 8.5. Additional contaminants were removed by size-exclusion chromatography with a HiLoad 16/600 Superdex 75 column. Protein purity was assessed by sodium dodecyl-sulfate polyacrylamide gel electrophoresis (SDS-PAGE), and the concentration of MIF-2 (expressed per monomer) was determined using $\epsilon_{280} = 5500 \; \text{M}^{-1} \; \text{cm}^{-1}$ and a Pierce Bicinchoninic Acid Protein Assay Kit (Thermo Fisher Scientific).

5.2 | NMR spectroscopy

Isotopically labeled NMR samples of MIF-2 were prepared as described earlier, but rather than LB medium, MIF-2 expression was carried out in M9 minimal media containing MEM vitamins (Sigma-Aldrich) and ¹⁵NH₄Cl (Cambridge Isotope Labs) as the sole nitrogen source. Purified MIF-2 was dialyzed into a final NMR buffer of 20 mM Tris, 20 mM NaCl at pH 7.4 with 10% D₂O and then concentrated to 0.5–1.0 mM. NMR experiments were performed on a Bruker Avance NEO 600 MHz spectrometer at 30°C. NMR data were processed using NMRPipe and analyzed in Sparky along with in-house scripts (Delaglio et al., 1995; Lee et al., 2015).

5.3 | Ebselen titrations of ¹⁵N-MIF-2

 $^{1}\text{H-}^{15}\text{N}$ TROSY HSQC fingerprint spectra of 0.5 mM MIF-2 were collected at 30°C in 20 mM Tris and 20 mM NaCl at pH 7.4 with 10% D $_{2}$ O. Ebselen (Focus Biomolecules) was dissolved in 100% DMSO-d $_{6}$ at a stock concentration of 200 mM. Titrations were performed by adding small aliquots of Ebselen to the MIF-2 sample with gentle mixing by pipette and a 1 h incubation time before the acquisition of spectra. Saturation of MIF-2 was followed until NMR chemical shift perturbations were no longer visible with subsequent additions of Ebselen. NMR chemical shift perturbations were quantified using the method of Bax and coworkers (Grzesiek et al., 1996).

5.4 | NMR spin relaxation

TROSY-based spin relaxation experiments were performed with the ^1H and ^{15}N carriers set to the water resonance and 120 ppm, respectively. Longitudinal relaxation rates (R_1) were measured with randomized T_1 delays of 0, 20, 60, 100, 200, 600, 800, 1200, 1500, 2000, and 2500 ms. Transverse relaxation rates (R_2) were measured with randomized T_2 delays of 0, 16.9, 33.9, 67.8, 136, 169, and 203 ms. Relaxation data were collected in a temperature-compensated interleaved

manner with eight scans of 10 and 256 points in the direct and indirect dimensions, respectively, over a 14 ppm 1 H and 35 ppm 15 N spectral width. The recycle delay in these experiments was 2.5 s (Zhu et al., 2000). Longitudinal and transverse relaxation rates were extracted by nonlinear least squares fitting of the peak heights to a single exponential decay using in-house software. Uncertainties in these rates were determined from replicate spectra with duplicate relaxation delays of 20 (×2), 60, 200, 600 (×2), 800, and 1200 ms for T_1 and 16.9, 33.9 (×2), 67.8, 136 (×2) and 203 ms for T_2 . The values of rotational correlation times (τ_c) were estimated using the following equation, where ν_N is the 15 N frequency in Hertz (Zhao et al., 2022):

$$\tau_c = \frac{1}{4\pi\nu_N} \sqrt{6\frac{R_2}{R_1} - 7}$$

5.5 | Solvent PRE

¹H-¹⁵N TROSY HSQC spectra of 0.5 mM MIF-2 were collected at 30°C in a buffer of 20 mM Tris and 20 mM NaCl at pH 7.4 with 10% D₂O. 4-Hydroxy-2,-2,6,6-tetramethylpiperidine-1-oxyl (TEMPOL, Fisher Scientific) was dissolved in the same buffer at a stock concentration of 5 M. sPRE titrations were carried out by adding increasing amounts of TEMPOL to the MIF-2 NMR sample to a final ratio of 1:40 (MIF-2:TEMPOL), reflecting the maximum decrease in NMR peak intensity. Ebselen was added to an identical NMR sample of MIF-2, incubated at room temperature for 1 h, and TEMPOL was again titrated to a ratio of 1:40 (MIF-2: TEMPOL). Data were analyzed based on the relationship of TEMPOL-saturated MIF-2 versus MIF-2 alone $(MIF-2_{tempol}/MIF-2_{apo} \text{ or } MIF-2 + Ebselen_{tempol}/MIF-2$ + Ebselen_{apo}).

5.6 | Liquid chromatography-mass spectroscopy

MIF-2 protein samples (WT, C23S, C56S, and C23S/C56S variants \pm Ebselen) were processed using S-Trap Micro columns (Protifi) with modified protocols (Waløen et al., 2021; Xie et al., 2022). Samples (50 μ g each) were lysed in sodium dodecyl sulfate/triethylammonium bicarbonate (SDS/TEAB) buffer, vortexed, and brought to

100 μL total volume. In one experiment, samples were neither reduced nor alkylated, while in another, samples were alkylated with 20 mM iodoacetamide for 30 min at room temperature. All samples were acidified, bound to S-Trap columns with methanol/TEAB, washed, and digested with 1 µg of trypsin per sample overnight at 37°C. In one experiment, pepsin was added prior to trypsin digestion for dual-enzyme processing. Peptides were sequentially eluted with water +0.1% formic acid (hydrophilic) and 50% acetonitrile (hydrophobic), vacuum-dried, and reconstituted. For both experiments, peptides were analyzed using a QExactive Orbitrap system with a 120-min gradient and Top9 DDA method, scanning from 400 to 1800 m/z with full MS resolution of 70,000 and MS/MS at 17,500. Peptides were separated using trapelute setups in all systems, and methods were optimized for identification of Ebselen-modified cysteines and disulfide-bonded peptides.

Raw MS data were analyzed using SpectroMine (v4.4.240326), FragPipe/MSFragger (v22.0/4.1), and Protein Metrics Byos (v5.9.125) with customized parameters to identify and characterize peptides, including Ebselen-cysteine adducts. SpectroMine searches were performed against the DOPD HUMAN UniProt reference (Purslow et al., 2020), 230316 release, including isoforms, using a 1% FDR for peptide and protein identification, with variable modification for Ebselen bound to cysteine (+273.973 Da) and an increased PTM localization probability threshold of 0.9. FragPipe/MSFragger searches used a custom database containing WT and variant MIF sequences (C23S, C56S, and C23S/C56S) appended to the E. coli proteome. Precursor and fragment tolerances were set at 50 ppm, and searches allowed no miscleavages, with variable modifications including methiooxidation and Ebselen (+273.9732 Da). IonQuant was used with match-between-runs and intensity normalization disabled, and deisotoping turned off. For combined pepsin/trypsin-digested samples. Byos searches used semi-specific digestion rules allowing cleavage after F, L, W, Y, R, and K with up to three missed cleavages. Precursor mass tolerance was set to 6-10 ppm, and one Ebselen modification (+275 Da) per cysteine residue was permitted. All search engines utilized default settings where applicable, with targeted modifications to accommodate the analysis of Ebselen-protein adducts and disulfide bond disruptions in mutant MIF samples. The percent modification of each peptide was determined as:



5.7 | Circular dichroism spectroscopy

Circular dichroism data were collected on a Jasco J-815 spectropolarimeter using a 0.2-cm quartz cuvette with 10 μm MIF-2 in a buffer of 20 mM sodium phosphate at pH 7.4. Thermal denaturation experiments were collected at 218 nm over a temperature range of 25–90°C, sampling 1.5°C at a rate of 1.5°C/min. Thermal unfolding profiles were fit to the following equation in GraphPad Prism:

Ellipticity(T)

$$=\frac{\left[\left(m_{f}T+b_{f}\right)+\left(m_{u}T+b_{u}\right)\right]\exp\left[\left(-\frac{\Delta H_{D,vH}}{R}\right)\left(\frac{1}{T}-\frac{1}{T_{m}}\right)\right]}{1+exp\left[\left(-\frac{\Delta H_{D,vH}}{R}\right)\left(\frac{1}{T}-\frac{1}{T_{m}}\right)\right]}$$

5.8 | Molecular dynamics simulations

The 1.27 Å resolution crystal structure of human MIF-2 (PDB ID: 7MSE) was aligned to the 2.60 Å MIF structure (PDB ID: 1MIF) and used as the receptor for docking. The pre-reaction form of Ebselen (ring closed) was docked to MIF-2 using AutoDock Vina (Trott & Olson, 2010) via UCSF Chimera (Pettersen et al., 2004). Among the top 10 predicted binding poses, the one closest to Cys23—the proposed binding site—was selected as the representative binding pose for subsequent molecular dynamics (MD) simulations. The postreaction form of Ebselen (ring-opened) was covalently docked to MIF-2 with AutoDockTools from the MGLTools package (Morris et al., 2009), yielding a pose closely matching the top binding pose of the prereaction form. The Ebselen parameters and topology were obtained from the Automated Topology Builder (ATB) repository (Malde et al., 2011) and converted to AMBER format. Bond and angle parameters for the Cys-Ebselen adduct were derived from an optimized structure at the B3LYP/6-31G(d,p) level for standard atoms and cc-pVTZ for sulfur and selenium using Gaussian16 (Frisch et al., 2016). Dihedral parameters for the selenium-sulfur bond were adopted from disulfide bond parameters in the AMBER GAFF2 library (Wang et al., 2004). MIF-2 parameters were generated using the tLEaP program from the AmberTools suite (Case et al., 2023, 2025). Initial preparation of the MIF-2 structure for MD simulations was performed using Schrödinger Maestro (2025)—the protein termini were capped, protonation states were predicted with PropKa (Olsson et al., 2011), and the structure was minimized using the OPLS force field (Jorgensen & Tirado-Rives, 1988) with a 0.3 Å RMSD restraint.

Two MD simulations were conducted: one with prereaction Ebselen unbound, but proximal to MIF-2, and one with a post-reaction Ebselen product covalently bound to Cvs23. Given the trimeric nature of MIF-2. three Ebselen molecules were docked at the corresponding sites in each monomer. The resulting complexes were solvated in a TIP3P water box (Klein et al., 1983) with a 15 Å buffer, and Na⁺ and Cl⁻ ions were added to neutralize each system at a physiological salt concentration of 0.15 M. MD simulations were performed using NAMD (Phillips et al., 2005). To mimic the formation of a selenium-sulfur covalent bond in the pre-reaction system, a harmonic restraint (2.23 Å. 388.24 kcal/mol/Å²) was applied between the selenium atom of Ebselen and the sulfur atom of Cys23. The systems underwent a three-step equilibration: [1] relaxation of solvent only, [2] relaxation of solvent and side chains, and [3] relaxation of the entire system. Hydrogen mass repartitioning (Hopkins et al., 2015) was applied to enable a 4 fs time step. Production MD simulations were run for 400 ns, while a parallel MD simulation of apo MIF-2 (no Ebselen bound) was performed under identical conditions for comparison. The X-ray maps were calculated from apo and pre-reaction MD simulations using the sfall program in CCP4 (Winn et al., 2011), and the corresponding structures were then fitted to the maps to obtain the equilibrated structures. ProLif (Bouysset & Fiorucci, 2021) was employed to analyze the protein-ligand interactions, and the results were visualized using PyMOL (DeLano, 2002).

5.9 | Enzymatic assays

MIF-2 activity was measured using a 100 mM stock solution of 4-hydroxyphenyl pyruvate (4-HPP) substrate, prepared in 500 mM ammonium acetate at pH 6.0 and rocked overnight to generate its keto form (Leng et al., 2003). MIF-2 enzymatic activity was determined by monitoring the increase in absorbance at 306 nm caused by enol-borate complex formation between boric acid and 4-HPP in the reaction solution. Absorbance was first recorded with a mixture of 1.2 mM 4-HPP and 420 mM boric acid; then the reaction was initiated by adding MIF-2 at a final concentration of 80 nM, and the absorbance was recorded during incubation for 3.5 min. To assess the inhibitory effect of Ebselen, the compound was first incubated with MIF-2 for 1 h at room temperature. Absorbance of a "blank" sample was first recorded with a mixture of 1.2 mM 4-HPP, 420 mM boric acid, and 160 nM Ebselen. The reaction was monitored by adding MIF-2 incubated with Ebselen to a fresh solution of 420 mM boric acid and 1.2 mM 4-HPP, and the absorbance was recorded during incubation for 3.5 min. A control experiment was conducted using the same volume of DMSO used to solubilize Ebselen, but in the absence of the Ebselen molecule.



5.10 | Spin-down assays

To quantify the percentage of MIF-2 precipitated from solution by Ebselen, 1 mL of 25 µM MIF-2 in a buffer of 20 mM Tris and 20 mM NaCl at pH 7.4 was centrifuged at 14.600 rpm for 5 mins at room temperature. The soluble fraction was separated from any precipitate with a micropipette. Then, the absorbance of the soluble fraction was measured at 280 nm using $\varepsilon_{280} = 10,500$ M⁻¹ cm⁻¹, accounting for the molar extinction coefficient of Ebselen (Zhao & Holmaren, 2002) to determine the amount of MIF-2 present at 0 h (initial reading), 6 h, 12 h, and 24 h after the addition of Ebselen at stoichiometric molar equivalence. A blank containing only buffer and the equivalent concentration of Ebselen was used for background correction. The assay was also carried out with 25 µM MIF-2 protein alone and MIF-2 protein with the same volume of DMSO used to solubilize Ebselen, which served as controls.

5.11 | Neutrophil recruitment assays

Wild-type adult male mice (10-12 weeks old) of genetic background strain C57BL6/J were purchased from Jackson Laboratory (Bar Harbor, ME) and housed in a pathogen-free animal facility at Cooper University Hospital, Camden, NJ, USA. Mice were administered a one-time intra-tracheal instillation of 50 µL of normal saline alone (vehicle) or 1 µg of either (1) Ebselen alone, (2) WT MIF-2, (3) C56S MIF-2, or (4) MIF-2-Ebselen complex, resuspended in 50 μL of DMSO and normal saline. MIF-2-Ebselen complexes were preformed and isolated from any remaining free Ebselen ligand via dialysis prior to administration to mice. Intratracheal instillation followed the methodology described in prior work (Parkins, Chen, et al., 2023). The mice were sacrificed after 6 h to collect BAL and estimate the total protein content in the BAL fluid by BCA assay (Thermo Scientific, Rockford, IL). Approximately 1 mL of the BAL fluid was pelleted at 1000 rpm for 10 min at 4°C. The pellet was resuspended in 200 μL of 1X PBS, and cytocentrifuged at 1000 rpm for 10 min at room temperature to spread the pellet evenly on slides as a smear. The slides were air dried and stained with Hema III differential Quick stain (Fisher Scientific, Cat. No. 122-911). The total percentage of neutrophils in the smears was determined manually following previously published methodology (De Brauwer et al., 2002; De Lorenzi et al., 2009). Briefly, following staining, the cytosmear was randomly divided into 4-5 areas that housed the maximum number of neutrophils. Two hundred different inflammatory cell types (including neutrophils) were counted in these areas, from which the percentage of neutrophils was calculated. At least 4-5 mice were used for the different groups of samples instilled. This animal study protocol was approved by

the Institutional Animal Care and Use Committee of Cooper University Hospital, Camden, NJ, USA. Statistical analysis was done in GraphPad Prism 8.4.3 by oneway ANOVA with Tukey's post-hoc correction, as

AUTHOR CONTRIBUTIONS

appropriate.

Vinnie Widjaja: Investigation; writing - original draft; writing - review and editing; formal analysis; funding acquisition. Sirena M. D'Orazio: Investigation; writing - original draft; formal analysis. Pragnya Das: Investigation; writing - original draft; writing - review and editing; formal analysis. Divya T. Rajendran: Investigation; formal analysis. Xander Takada: Investigation; formal analysis. Yuanjun Shi: Investigation; writing - original draft; formal analysis. Iz Varghese: Investigation; formal analysis. Yannie Lam: Investigation; formal analysis. Nicholas DaSilva: Investigation; formal analysis. Jimin Wang: Writing - review and editing; formal analysis. Victor S. Batista: Supervision; writing - review and editing; funding acquisition. Vineet Bhandari: Writing - review and editing; supervision; project administration; funding acquisition. George P. Lisi: Funding acquisition; writing - review and editing; supervision; project administration.

ACKNOWLEDGMENTS

This work was supported by NIH grant R01 GM144451 (to GPL, VSB, and VB). VW was supported by NSF GRFP Grant 2040433. The Proteomics Core Facility, which was supported in part by the National Institutes of Health Grant No. 1S10RR027027 (Orbitrap XL-ETD), 1S10OD036295 (Ascend Tribrid, FAIMS, Vanquish Neo), and the Division of Biology and Medicine, Brown University.

CONFLICT OF INTEREST STATEMENT

The authors declare no conflicts of interest.

DATA AVAILABILITY STATEMENT

NMR assignments of MIF-2 have previously been deposited under BMRB entry 50,790. All other data is available from the corresponding author upon request.

ORCID

Jimin Wang https://orcid.org/0000-0002-4504-8038 George P. Lisi https://orcid.org/0000-0001-8878-5655

REFERENCES

Al-Abed Y, Dabideen D, Aljabari B, Valster A, Messmer D, Ochani M, et al. ISO-1 binding to the tautomerase active site of MIF inhibits its pro-inflammatory activity and increases survival in severe sepsis. J Biol Chem. 2005;280(44):36541–4.

Capper MJ, Wright GSA, Barbieri L, Luchinat E, Mercatelli E, McAlary L, et al. The cysteine-reactive small molecule ebselen facilitates effective SOD1 maturation. Nat Commun. 2018;9(1): 1693.



- Case DA, Aktulga HM, Belfon K, Ben-Shalom IY, Berryman JT, Brozell SR, et al. AMBER. San Francisco: University of California; 2025.
- Case DA, Aktulga HM, Belfon K, Cerutti DS, Cisneros GA, Cruzeiro VWD, et al. AmberTools. J Chem Inf Model. 2023; 63(20):6183–91.
- Chen E, Reiss K, Shah D, Manjula R, Allen B, Murphy EL, et al. A structurally preserved allosteric site in the MIF superfamily affects enzymatic activity and CD74 activation in D-dopachrome tautomerase. J Biol Chem. 2021;297(3):101061.
- Chen E, Widjaja V, Kyro G, Allen B, Das P, Prahaladan VM, et al. Mapping N- to C-terminal allosteric coupling through disruption of a putative CD74 activation site in D-dopachrome tautomerase. J Biol Chem. 2023;299(6):104729.
- Cho Y, Crichlow GV, Vermeire JJ, Leng L, Du X, Hodsdon ME, et al. Allosteric inhibition of macrophage migration inhibitory factor revealed by ibudilast. Proc Natl Acad Sci USA. 2010;107(25): 11313–8.
- Coleman AM, Rendon BE, Zhao M, Qian MW, Bucala R, Xin D, et al. Cooperative regulation of non-small cell lung carcinoma angiogenic potential by macrophage migration inhibitory factor and its homolog, D-dopachrome tautomerase. J Immunol. 2008;181(4): 2330–7
- Cooke G, Armstrong ME, Donnelly SC. Macrophage migration inhibitory factor (MIF), enzymatic activity and the inflammatory response. Biofactors. 2009;35(2):165–8.
- de Brauwer El, Jacobs JA, Nieman F, Bruggeman CA, Drent M. Bronchoalveolar lavage fluid differential cell count. How many cells should be counted? Anal Quant Cytol Histol. 2002;24(6): 337–41.
- de Lorenzi D, Masserdotti C, Bertoncello D, Tranquillo V. Differential cell counts in canine cytocentrifuged bronchoalveolar lavage fluid: a study on reliable enumeration of each cell type. Vet Clin Pathol. 2009;38(4):532–6.
- Delaglio F, Grzesiek S, Vuister GW, Zhu G, Pfeifer J, Bax A. NMRPipe: a multidimensional spectral processing system based on UNIX pipes. J Biomol NMR. 1995;6(3):277–93.
- DeLano WL. PyMOL: an open-source molecular graphics tool. CCP4 Newsletter Protein Crystallogr. 2002;40:82–9.
- Fan C, Rajasekaran D, Syed MA, Leng L, Loria JP, Bhandari V, et al. MIF intersubunit disulfide mutant antagonist supports activation of CD74 by endogenous MIF trimer at physiologic concentrations. Proc Natl Acad Sci USA. 2013;110(27):10994–9.
- Feng Q, Li X, Sun W, Li Y, Yuan Y, Guan B, et al. Discovery of Ebselen as an inhibitor of 6PGD for suppressing tumor growth. Cancer Manag Res. 2020;12:6921–34.
- Frisch MJ, Trucks GW, Schlegel HB, Scuseria GE, Robb MA, Cheeseman JR, et al. Gaussian 16 Revision C.01. Wallingford, CT: Gaussian, Inc.; 2016.
- Grzesiek S, Stahl SJ, Wingfield PT, Bax A. The CD4 determinant for downregulation by HIV-1 Nef directly binds to Nef. Mapping of the Nef binding surface by NMR. Biochemistry. 1996;35(32): 10256–61.
- Hopkins CW, Le Grand S, Walker RC, Roitberg AE. Long-time-step molecular dynamics through hydrogen mass repartitioning. J Chem Theory Comput. 2015;11(4):1864–74.
- Jorgensen WL, Tirado-Rives J. The OPLS [optimized potentials for liquid simulations] potential functions for proteins, energy minimizations for crystals of cyclic peptides and crambin. J Am Chem Soc. 1988;110(6):1657–66.
- Kay LE, Torchia DA, Bax A. Backbone dynamics of proteins as studied by 15N inverse detected heteronuclear NMR spectroscopy: application to staphylococcal nuclease. Biochemistry. 1989; 28(23):8972–9.
- Klein ML, Jorgensen WL, Chandrasekhar J, Madura JD, Impey RW. Comparison of simple potential functions for simulating liquid wate. J Chem Phys. 1983;79:926–36.

- Landgraf AD, Alsegiani AS, Alaqel S, Thanna S, Shah ZA, Sucheck SJ. Neuroprotective and anti-neuroinflammatory properties of Ebselen derivatives and their potential to inhibit neurodegeneration. ACS Chem Nerosci. 2020;11(19):3008–16.
- Lee W, Tonelli M, Markley JL. NMRFAM-SPARKY: enhanced software for biomolecular NMR spectroscopy. Bioinformatics. 2015; 31(8):1325–7.
- Leng L, Metz CN, Fang Y, Xu J, Donnelly S, Baugh J, et al. MIF signal transduction initiated by binding to CD74. J Exp Med. 2003; 197(11):1467–76.
- Lisi GP, Loria JP. Solution NMR spectroscopy for the study of enzyme allostery. Chem Rev. 2016;116(11):6323–69.
- Lubetsky JB, Dios A, Han J, Aljabari B, Ruzsicska B, Mitchell R, et al. The tautomerase active site of macrophage migration inhibitory factor is a potential target for discovery of novel anti-inflammatory agents. J Biol Chem. 2002;277(28):24976–82.
- Malde AK, Zuo L, Breeze M, Stroet M, Poger D, Nair PC, et al. An automated force field topology builder (ATB) and repository: version 1.0. J Chem Theory Comput. 2011;7(12):4026–37.
- Merk M, Mitchell RA, Endres S, Bucala R. D-dopachrome tautomerase (D-DT or MIF-2): doubling the MIF cytokine family. Cytokine. 2012;59(1):10–7.
- Morris GM, Huey R, Lindstrom W, Sanner MF, Belew RK, Goodsell DS, et al. AutoDock4 and AutoDockTools4: automated docking with selective receptor flexibility. J Comput Chem. 2009; 30(16):2785–91.
- Olsson MH, Søndergaard CR, Rostkowski M, Jensen JH. PROPKA3: consistent treatment of internal and surface residues in empirical pKa predictions. J Chem Theory Comput. 2011;7(2):525–37.
- Ouertatani-Sakouhi H, El-Turk F, Fauvet B, Cho MK, Pinar Karpinar D, Le Roy D, et al. Identification and characterization of novel classes of macrophage migration inhibitory factor (MIF) inhibitors with distinct mechanisms of action. J Biol Chem. 2010; 285(34):26581–98.
- Pantouris G, Bucala R, Lolis EJ. Structural plasticity in the C-terminal region of macrophage migration inhibitory Factor-2 is associated with an induced fit mechanism for a selective inhibitor. Biochemistry. 2018;57(26):3599–605.
- Pantouris G, Syed MA, Fan C, Rajasekaran D, Cho TY, Rosenberg EM Jr, et al. An analysis of MIF structural features that control functional activation of CD74. Chem Biol. 2015; 22(9):1197–205.
- Parkins A, Chen E, Rangel VM, Singh M, Xue L, Lisi GP, et al. Ligand-induced conformational changes enable intersubunit communications in D-dopachrome tautomerase. Biophys J. 2023:122:1268–76.
- Parkins A, Das P, Prahaladan V, Rangel VM, Xue L, Sankaran B, et al. 2,5-Pyridinedicarboxylic acid is a bioactive and highly selective inhibitor of D-dopachrome tautomerase. Structure. 2023;31(3):355–367.e4.
- Parkins A, Skeens E, McCallum CM, Lisi GP, Pantouris G. The N-terminus of MIF regulates the dynamic profile of residues involved in CD74 activation. Biophys J. 2021;120(18):3893–900.
- Pettersen EF, Goddard TD, Huang CC, Couch GS, Greenblatt DM, Meng EC, et al. UCSF chimera—a visualization system for exploratory research and analysis. J Comput Chem. 2004; 25(13):1605–12.
- Phillips JC, Braun R, Wang W, Gumbart J, Tajkhorshid E, Villa E, et al. Scalable molecular dynamics with NAMD. J Comput Chem. 2005;26(16):1781–802.
- Purslow JA, Khatiwada B, Bayro MJ, Venditti V. NMR methods for structural characterization of protein–protein complexes. Front Mol Biosci. 2020;7:9.
- Sajko S, Skeens E, Schinagl A, Ferhat M, Mirkina I, Mayer J, et al. Redox-dependent plasticity of oxMIF facilitates its interaction with CD74 and therapeutic antibodies. Redox Biol. 2024;75: 103264.



- Schinagl A, Kerschbaumer RJ, Sabarth N, Douillard P, Scholz P, Voelkel D, et al. Role of the cysteine 81 residue of macrophage migration inhibitory factor as a molecular redox switch. Biochemistry. 2018;57(9):1523–32.
- Schinagl A, Thiele M, Douillard P, Völkel D, Kenner L, Kazemi Z, et al. Oxidized macrophage migration inhibitory factor is a potential new tissue marker and drug target in cancer. Oncotarget. 2016;7(45):73486–96.
- Bouysset C Fiorucci S. ProLif: A library to encode molecular interactions as fingerprints. J. Cheminformatics. 2021;13(72):1–9.
- Schrödinger, LLC. 2 SR. New York, NY 2025.Maestro
- Shi X, Leng L, Wang T, Wang W, Du X, Li J, et al. CD44 is the signaling component of the macrophage migration inhibitory factor-CD74 receptor complex. Immunity. 2006;25(4): 595–606.
- Skeens E, Gadzuk-Shea M, Shah D, Bhandari V, Schweppe DK, Berlow RB, et al. Redox-dependent structure and dynamics of macrophage migration inhibitory factor reveal sites of latent allostery. Structure. 2022;30(6):840–850.e6.
- Skeens E, Pantouris G, Shah D, Manjula R, Ombrello MJ, Maluf NK, et al. A cysteine variant at an allosteric site alters MIF dynamics and biological function in homo- and heterotrimeric assemblies. Front Mol Biosci. 2022;9:783669.
- Song S, Xiao Z, Dekker FJ, Poelarends GJ, Melgert BN. Macrophage migration inhibitory factor family proteins are multitasking cytokines in tissue injury. Cell Mol Life Sci. 2022;79(2):105.
- Su XC, Jergic S, Ozawa K, Burns ND, Dixon NE, Otting G. Measurement of dissociation constants of high-molecular weight proteinprotein complexes by transferred 15N-relaxation. J Biomol NMR. 2007;38(1):65–72.
- Thiele M, Bernhagen J. Link between macrophage migration inhibitory factor and cellular redox regulation. Antioxid Redox Signal. 2005;7(9–10):1234–48.
- Tilstam PV, Pantouris G, Corman M, Andreoli M, Mahboubi K, Davis G, et al. A selective small-molecule inhibitor of macrophage migration inhibitory factor-2 (MIF-2), a MIF cytokine superfamily member, inhibits MIF-2 biological activity. J Biol Chem. 2019;294(49):18522–31.
- Tilstam PV, Schulte W, Holowka T, Kim BS, Nouws J, Sauler M, et al. MIF but not MIF-2 recruits inflammatory macrophages in an experimental polymicrobial sepsis model. J Clin Invest. 2021; 131(23): e127171–86.
- Trivedi-Parmar V, Jorgensen WL. Advances and insights for small molecule inhibition of macrophage migration inhibitory factor. J Med Chem. 2018;61(18):8104–19.
- Trott O, Olson AJ. AutoDock Vina: improving the speed and accuracy of docking with a new scoring function, efficient optimization, and multithreading. J Comput Chem. 2010;31(2):455–61.
- Waløen K, Jung-Kc K, Vecchia ED, Pandey S, Gasparik N, Døskeland A, et al. Cysteine modification by Ebselen reduces the stability and cellular levels of 14-3-3 proteins. Mol Pharmacol. 2021;100(2):155–69.

- Wand AJ, Sharp KA. Measuring entropy in molecular recognition by proteins. Annu Rev Biophys. 2018;47:41–61.
- Wang J, Wolf RM, Caldwell JW, Kollman PA, Case DA. Development and testing of a general AMBER force field. J Comput Chem. 2004;25(9):1157–74.
- Winn MD, Ballard CC, Cowtan KD, Dodson EJ, Emsley P, Evans PR, et al. Overview of the CCP4 suite and current developments. Acta Crystallogr D Biol Crystallogr. 2011;67(Pt 4):235–42.
- Winner M, Meier J, Zierow S, Rendon BE, Crichlow GV, Riggs R, et al. A novel, macrophage migration inhibitory factor suicide substrate inhibits motility and growth of lung cancer cells. Cancer Res. 2008;68(18):7253–7.
- Xiao Z, Osipyan A, Song S, Chen D, Schut RA, van Merkerk R, et al. Thieno[2,3-d]pyrimidine-2,4(1H,3H)-dione derivative inhibits d-dopachrome tautomerase activity and suppresses the proliferation of non-small cell lung cancer cells. J Med Chem. 2022; 65(3):2059–77.
- Xie H, Qiang P, Wang Y, Xia F, Liu P, Li M. Discovery and mechanism studies of a novel ATG4B inhibitor Ebselen by drug repurposing and its anti-colorectal cancer effects in mice. Cell Biosci. 2022;12(1):206.
- Zhao R, Holmgren A. A novel antioxidant mechanism of ebselen involving ebselen diselenide, a substrate of mammalian thioredoxin and thioredoxin reductase. J Biol Chem. 2002;277(42):39456–62.
- Zhao R, Masayasu H, Holmgren A. Ebselen: a substrate for human thioredoxin reductase strongly stimulating its hydroperoxide reductase activity and a superfast thioredoxin oxidant. Proc Natl Acad Sci USA. 2002;99(13):8579–84.
- Zhao Y, Hu J, Yang SS, Zhong J, Liu J, Wang S, et al. A redox switch regulates the assembly and anti-CRISPR activity of AcrIIC1. Nat Commun. 2022;13(1):7071.
- Zhu G, Xia Y, Nicholson LK, Sze KH. Protein dynamics measurements by TROSY-based NMR experiments. J Magn Reson. 2000;143(2):423–6.

SUPPORTING INFORMATION

Additional supporting information can be found online in the Supporting Information section at the end of this article.

How to cite this article: Widjaja V, D'Orazio SM, Das P, Rajendran DT, Takada X, Shi Y, et al. Atomistic modulation of MIF-2 structure, catalysis, and biological signaling via cysteine residues and a small molecule, Ebselen. Protein Science. 2025;34(11):e70344. https://doi.org/10.1002/pro.70344